Journal of Integrative Neuroscience

J. Integr. Neurosci. **2026**; 25(9): 51769
https://doi.org/10.31083/JIN51769

Original Research

SPATA2 Attenuates Inflammatory Injury Through CYLD-Related Regulation of Microglial Inflammatory Responses After Focal Cerebral Ischemia/Reperfusion in Rats

Jin Jiang[1,2], Xingrui Li[3], Yexiang Du[4], Yehong Du[5,*], Wei Yu[2,5,*]

[1]Department of Rehabilitation Medicine, Key Laboratory of Physical Medicine and Precision Rehabilitation of Chongqing Municipal Health Commission, The First Affiliated Hospital of Chongqing Medical University, 400010 Chongqing, China
[2]Laboratory Research Center, The First Affiliated Hospital of Chongqing Medical University, 400016 Chongqing, China
[3]Department of Medicine (School of Physical Education and Health), Chongqing College of Humanities, Science & Technology, 400010 Chongqing, China
[4]Center for Neuroscience Research, School of Basic Medical Sciences, Institute for Brain Science and Disease, Department of Anatomy, School of Basic Medical Sciences, Chongqing Medical University, 400016 Chongqing, China
[5]Pediatric Research Institute, Ministry of Education Key Laboratory of Child Development and Disorders, National Clinical Research Center for Children and Adolescents' Health and Diseases, Chongqing Key Laboratory of Child Neurodevelopment and Cognitive Disorders, Department of Anesthesiology, Children's Hospital of Chongqing Medical University, 400014 Chongqing, China
*Correspondence: yehongdu@foxmail.com (Yehong Du); yuwei3272@163.com (Wei Yu)
Academic Editors: Hahn Young Kim and Bettina Platt
Submitted: 11 March 2026 Revised: 3 July 2026 Accepted: 20 July 2026 Published: 21 September 2026

Abstract

Background: Post-ischemic inflammation is strongly influenced by interactions between neurons and microglia. We previously observed that spermatogenesis-associated protein 2 (SPATA2) alleviates inflammatory injury following cerebral ischemia/reperfusion; however, the relationship between SPATA2, cylindromatosis (CYLD)-associated inflammatory signaling, and microglial inflammatory responses remains incompletely understood. **Methods:** Adult Sprague-Dawley (SD) rats were subjected to transient middle cerebral artery occlusion followed by reperfusion. SPATA2 expression was knocked down *in vivo* via intracerebroventricular lentiviral delivery. Neurological function and infarct volume were evaluated after reperfusion. Selected pro-inflammatory and anti-inflammatory/reparative markers were assessed by immunofluorescence, real-time quantitative polymerase chain reaction (RT-qPCR), and enzyme-linked immunosorbent assay (ELISA). Double immunofluorescence staining of SPATA2 with neuronal nuclei (NeuN), ionized calcium-binding adapter molecule 1 (Iba1), or glial fibrillary acidic protein (GFAP) was performed to examine the cellular localization of SPATA2 in the peri-ischemic cortex. To further assess neuron-to-microglia regulation, primary neurons and microglia were cultured in a Transwell system and exposed to oxygen-glucose deprivation/reperfusion. SPATA2 knockdown and overexpression, together with CYLD knockdown in SPATA2-overexpressing cells, were used to investigate CYLD-associated signaling. Co-immunoprecipitation (Co-IP) was performed to assess CYLD-heme-oxidized IRP2 ubiquitin ligase 1L-like interacting protein (HOIP) association. **Results:** SPATA2 knockdown exacerbated neurological deficits and increased infarct volume following middle cerebral artery occlusion (MCAO). In peri-ischemic cortex tissue, SPATA2 knockdown increased the proportion of Iba1+/cluster of differentiation 86 (CD86)+ cells while reducing the proportion of Iba1+/CD206+ cells. Representative double-immunofluorescence images showed that SPATA2 immunoreactivity predominantly overlapped with NeuN-positive neurons, with relatively limited overlap with Iba1-positive microglia or GFAP-positive astrocytes. In the Transwell-based neuron–microglia system, depletion of SPATA2 in neurons shifted microglia toward a stronger inflammatory profile, as reflected by elevated secretion of interleukin-1 beta (IL-1β), IL-6, tumor necrosis factor alpha (TNF-α), and soluble C-X-C motif 3 chemokine ligand 1 (CX3CL1). By contrast, neuronal SPATA2 overexpression attenuated these inflammatory changes. At the mechanistic level, SPATA2 overexpression strengthened the association between CYLD and HOIP, together with reduced nuclear factor-κB (NF-κB) p65 expression and decreased soluble CX3CL1 release. When CYLD was silenced, the suppressive influence of SPATA2 overexpression on NF-κB p65 expression and soluble CX3CL1 release was partly weakened, indicating that CYLD contributes to this regulatory process. **Conclusion:** SPATA2 attenuates inflammatory injury following focal cerebral ischemia/reperfusion and modulates selected microglial inflammatory markers. *In vitro* results further support the role of neuron-derived SPATA2 in regulating microglial inflammatory responses in a Transwell co-culture system. Based on these observations, SPATA2 may be involved in CYLD-related inflammatory signaling and the regulation of CX3CL1/CX3C chemokine receptor 1 (CX3CR1) pathway activity.

Keywords: spermatogenesis-associated protein 2; cylindromatosis; microglia; neuroinflammation; brain ischemia; reperfusion injury; chemokine CX3CL1

Copyright: © 2026 The Author(s). Published by IMR Press.
This is an open access article under the CC BY 4.0 license.

Publisher's Note: IMR Press stays neutral with regard to jurisdictional claims in published maps and institutional affiliations.

1. Introduction

Ischemic stroke remains a leading cause of morbidity and mortality worldwide [1]. As the predominant form of stroke, acute ischemic stroke (AIS) is usually caused by thrombus-mediated blockage of cerebral arteries and often leads to neurological impairment [2]. Among AIS-related vascular occlusions, middle cerebral artery occlusion (MCAO) is especially severe, as it can produce extensive infarction and predispose patients to malignant cerebral edema, a complication linked to unfavorable prognosis [3]. AIS involves multiple pathological mechanisms, including neuroinflammation, excitotoxicity, Ca^{2+} overload, and oxidative stress. Neuroinflammation is orchestrated by chemokines and cytokines (e.g., tumor necrosis factor alpha (TNF-α) and interleukin-1 beta (IL-1β)) and involves complex crosstalk among multiple cell types, particularly neurons and microglia [4]. Clarifying how neurons and microglia interact after ischemic injury may help identify new targets for stroke intervention.

Under physiological conditions, microglia in the central nervous system (CNS) exhibit a quiescent, ramified morphology in the absence of external stimulation. As resident immune sentinels, they are essential for sensing insults and initiating repair processes to maintain neuronal homeostasis [5]. In response to external stimuli, microglia become activated and undergo dynamic morphological remodeling, thereby coordinating immune defense and facilitating lesion clearance; they also contribute to tissue homeostasis by removing cellular debris and denatured proteins [6]. Activated microglia can adopt diverse inflammatory phenotypes, which have traditionally been described using simplified pro-inflammatory/M1-like and anti-inflammatory/reparative/M2-like classifications [7,8]. Microglia can influence neuronal function by releasing cytokines, while neurons also shape microglial behavior through chemokine-mediated signaling. Among these neuronal cues, C-X-C motif 3 chemokine ligand 1 (CX3CL1) acts on CX3C chemokine receptor 1 (CX3CR1) expressed by microglia and thereby contributes to neuron–microglia communication [9,10,11]. The CX3CL1/CX3CR1 axis has also been linked to nuclear factor-κB (NF-κB)-dependent inflammatory signaling in different pathological settings [12,13]. Several studies have suggested that modulation of this signaling axis can alter neuron-microglia communication and influence inflammatory responses and tissue homeostasis [14,15].

Accumulating evidence indicates that cylindromatosis (CYLD), a deubiquitinase (DUB), acts as a negative regulator of inflammation, partly because it restrains NF-κB signaling activity [16,17]. For example, CYLD suppresses myeloid differentiation factor 88 (MyD88)-mediated signaling by removing K63-linked polyubiquitin chains from MyD88 [18]. Our earlier work showed that increased CYLD expression in the peri-infarct cortex limited excessive microglial activation and decreased the production of pro-inflammatory cytokines, accompanied by reduced NF-κB pathway activity [19]. CYLD is also known to interact with the linear ubiquitin chain assembly complex (LUBAC), thereby contributing to the suppression of LUBAC activity [20,21,22]. The LUBAC complex contains three core components: shank-associated RH domain interacting protein (SHARPIN), heme-oxidized IRP2 ubiquitin ligase 1L (HOIL-1L), and HOIL-1L interacting protein (HOIP), the catalytic E3 ligase subunit [23]. Spermatogenesis-associated protein 2 (SPATA2) functions as an adaptor that recruits CYLD to HOIP via its PNGase/UBA or UBX-containing proteins (PUB) domain [24]. Although initially described as widely expressed, SPATA2 shows the highest expression levels in the testis and brain [25]. We previously demonstrated that SPATA2 is predominantly expressed in cortical neurons in rats following ischemic stroke [26]. At the molecular level, SPATA2 serves as a linker between CYLD and HOIP. This linkage is mediated by the interaction of the SPATA2 PUB domain with the CYLD USP domain and with the PUB-interacting motif (PIM) of HOIP [27]. This interaction enhances the deubiquitinase activity of CYLD and modulates LUBAC signaling. For example, SPATA2 can promote the recruitment of CYLD, which contributes to the inhibition of NEK7-dependent NOD-like receptor family, pyrin domain-containing 3 (NLRP3) inflammasome activation [28]. In addition, SPATA2 has been linked to the control of NF-κB signaling [29]. In line with these observations, we previously found that reducing SPATA2 expression in the peri-ischemic cortex aggravated microglial activation in rats subjected to focal cerebral ischemia/reperfusion. This effect was associated with activation of the NF-κB/p38 pathway and the NLRP3 inflammasome [26]. It is still uncertain whether SPATA2 modulates specific microglial inflammatory markers after ischemic injury by acting through CYLD-related signaling and neuron–microglia communication.

Therefore, the present study was designed to define the role of SPATA2 in post-ischemic inflammatory injury and in the regulation of selected microglial inflammatory markers after focal cerebral ischemia/reperfusion. In addition, a Transwell neuron–microglia co-culture system was used to assess how neuron-derived SPATA2 affects microglial inflammatory responses, with emphasis on CYLD-related signaling and CX3CL1/CX3CR1 pathway activity.

2. Materials and Methods

2.1 Animals

For the *in vivo* MCAO experiments, 60 adult male Sprague-Dawley (SD) rats weighing 280–300 g were used. Postnatal day 1 SD pups were used for primary cortical neuron and microglial cultures. The animals were obtained from the Experimental Animal Center of Chongqing Medical University (Chongqing, China). Animals were housed at a 12 h light/dark schedule with a temperature of 20–24

℃ unrestricted access to chow and water. The reporting of this study follows the ARRIVE 2.0 guidelines, and the completed ARRIVE 2.0 checklist is provided in the **Supplementary Materials**.

2.2 Establishment of the Focal Cerebral Ischemia/Reperfusion Model

A transient focal cerebral ischemia/reperfusion model was generated by occluding the middle cerebral artery and subsequently restoring blood flow, with minor modifications to the previously reported procedure. Adult rats were anesthetized with pentobarbital sodium (60 mg/kg, i.p., Y0002194, Sigma-Aldrich, St. Louis, MO, USA). A nylon filament (MSRC40B200PK50, RWD, Shenzhen, Guangdong, China) was inserted via the right external carotid artery and advanced about 2.0 cm into the internal carotid artery until it blocked the origin of the middle cerebral artery. After 2 h of occlusion, reperfusion was initiated by gently withdrawing the filament. In the sham group, rats received identical surgical exposure, but the filament was not inserted.

During surgery, body temperature was maintained at 37.0–37.5 °C using a heating pad (69023, RWD, Shenzhen, Guangdong, China). After surgery, rats were monitored until recovery from anesthesia and then returned to temperature-controlled cages. After the rats recovered from anesthesia, neurological impairment was evaluated with the Longa scoring system [30] by an investigator who was unaware of the group assignments. Longa scores of 2 or 3 were used as prespecified inclusion criteria for successful MCAO. Animals with scores of 0 or 1 were excluded because of insufficient ischemic injury, whereas animals with a score of 4 were excluded because of excessive injury severity. Animals that died before the experimental endpoint or developed surgical complications such as subarachnoid hemorrhage were also excluded from the final analysis.

A total of 36 rats underwent MCAO surgery. Among them, 3 rats were excluded because of Longa scores of 0 or 1, 4 rats were excluded because of a Longa score of 4, 2 rats died before the experimental endpoint. The remaining animals were included for the following experiments.

Regional cerebral blood flow was not monitored by laser Doppler flowmetry in the present study. Therefore, ischemic injury was evaluated using prespecified neurological deficit criteria and was further confirmed by 2,3,5-triphenyltetrazolium chloride (TTC, T8877; Sigma-Aldrich) staining in the relevant experimental cohorts.

Unless otherwise indicated, rats were deeply anesthetized with pentobarbital sodium (60 mg/kg, i.p.) at 72 h after reperfusion, followed by transcardial perfusion as terminal euthanasia. Death was verified by cessation of heartbeat and respiration. Peri-ischemic cortical samples were harvested for molecular assays, whereas brain sections including this region were prepared for immunofluorescence analysis.

2.3 Lentivirus Production and Administration

Lentivirus administration was performed as previously described [19]. GeneChem (Shanghai, China) supplied the recombinant lentiviral vectors carrying either SPATA2-specific shRNA (LV-shSPATA2) or a non-targeting control sequence (lentiviral vector (LV)-scramble). The lentiviral construct was driven by a broad promoter and did not contain a fluorescent reporter. Therefore, the *in vivo* viral manipulation was not considered neuron-specific.

At 14 days before MCAO induction, 5 µL of LV-shSPATA2 or LV-scramble was administered into the right lateral ventricle at an infusion rate of 0.3 µL/min. The stereotaxic coordinates were as follows: 1.5 mm lateral to the midline, 1.1 mm posterior to bregma, and 3.8 mm below the skull surface. After completion of the infusion, the needle remained in position for an additional 5 min to reduce backflow. SPATA2 knockdown efficiency was verified by real-time quantitative polymerase chain reaction (RT-qPCR) and Western blotting in peri-ischemic cortical tissue.

2.4 Primary Microglial Cultures

A primary microglial culture was prepared as previously described, with some modifications [31]. Rats were also disinfected with 75% alcohol. Meninges were gently isolated from postnatal day 1 SD rats and incubated in 4 ℃ anatomical fluid (Hanks' balanced salt solution, HBSS, 14175095, Gibco, Grand Island, NY, USA). Tissues were chopped with scissors and digested with 1.5 mL of 0.25% trypsin (25200056; Gibco) at 37 ℃ for 20 min. Digestion was terminated by Dulbecco's modified Eagle's medium/F12 medium (DMEM/F12, 11320033, Gibco) supplemented with 10% fetal bovine serum (FBS, 10099141, Gibco). The cell suspension was then centrifuged at 900 rpm for 10 min, and the harvested cells were transferred to a humidified incubator (3111GP, Thermo Fisher Scientific, Waltham, MA, USA) containing 5% CO_2 for culture. After 3 h of incubation, the culture medium was refreshed to remove cell debris. Cells were fed every third day by replacement with fresh culture medium. After 2 weeks, in the mixed culture, astrocytes lay at the bottom, and microglia grew on top of the astrocytic layer. Microglial cells were isolated by shaking the culture vessels at 200 rpm for 4 h at 37 ℃. Cultured microglia were detected by ionized calcium-binding adaptor molecule 1 (Iba1; NB100-1028SS, Novus, Centennial, CO, USA, 1:50) immunocytochemical staining.

2.5 Primary Cortical Neuron Cultures

Postnatal day 1 rats were disinfected with 75% ethanol before surgery. Meningeal tissues from postnatal day 1

SD rats were carefully removed and promptly placed in HBSS (14175095, Gibco) pre-cooled to 4 °C. The tissues were chopped and digested with papain (P4762, Sigma-Aldrich) for 10–20 min. The enzymatic activity of papain was neutralized with DMEM/F12, followed by gentle trituration. The cell suspension was centrifuged at 1000 rpm for 5 min. The dissociated cells were seeded in poly-L-lysine-coated flasks (P4707, Sigma-Aldrich) containing DMEM/F12 with 10% FBS and were allowed to adhere for 6–8 h at 37 °C in a humidified 5% CO_2 atmosphere. After cell attachment, the medium was changed to Neurobasal medium containing 2% B27 (17504044; Gibco) and 0.5 mM glutamine (25030081, Gibco). Half of the medium was replaced with fresh medium every 3 days. Immunofluorescence staining was performed to identify cultured cells using an anti-neuronal nuclei (NeuN) antibody (MAB377, Millipore, Darmstadt, Germany; 1:200). The primary microglia and primary cortical neurons were tested for mycoplasma contamination using the Mycoplasma Detection Kit (PCR) (MedChemExpress, Monmouth Junction, NJ, USA, HY-K0552), both primary cell preparations were confirmed to be mycoplasma-negative. Primary cortical neurons were identified based on their characteristic neuronal morphology and positive NeuN immunofluorescence staining using an anti-NeuN antibody (MAB377, Millipore, 1:100, for neuron labeling).

2.6 Co-Culture

A Transwell neuron–microglia co-culture system was established to investigate neuron–microglia communication. Primary cortical neurons were seeded onto poly-L-lysine-coated plates or coverslips and cultured for 5 days. Primary microglia were then seeded into Transwell inserts at a neuron-to-microglia ratio of 2:1. This configuration allowed paracrine signaling between neurons and microglia without direct cell–cell contact.

For SPATA2 knockdown or overexpression experiments, primary neurons were transfected with si-SPATA2, siRNA negative control, pcDNA3.1-SPATA2, or empty pcDNA3.1 vector prior to the addition of microglia. After transfection, microglia were introduced to establish the Transwell co-culture system, which was maintained for 24 h before subsequent analyses.

For immunofluorescence quantification, multiple randomly selected microscopic fields were analyzed for each independent culture. Technical field values were averaged, and each independent neuronal preparation was considered a single biological replicate.

2.7 Oxygen-Glucose Deprivation/Reperfusion

Oxygen-glucose deprivation/reperfusion (OGD/R) was performed in the Transwell neuron–microglia co-culture system. Once the co-culture system had been established, the medium was changed to glucose-free D-Hanks' solution (8.0 g/L NaCl, 0.4 g/L KCl, 0.06 g/L KH_2PO_4, 0.06 g/L Na_2HPO_4, and 0.35 g/L $NaHCO_3$, pH 7.2–7.4). The cells were then exposed to an anaerobic environment consisting of 94% N_2, 1% O_2, and 5% CO_2 at 37 °C for 2 h. Reperfusion was initiated by replacing the glucose-free solution with normal culture medium, followed by incubation under normoxic conditions.

After reperfusion, neuronal lysates from the lower chamber were collected for Western blotting, whereas co-culture supernatants were collected for enzyme-linked immunosorbent assay (ELISA) analysis of soluble cytokines and soluble CX3CL1 (E-EL-R0385, Elabscience, Wuhan, Hubei, China). In this assay, the ELISA result represents soluble CX3CL1 in the culture supernatant rather than membrane-associated CX3CL1 or total cellular CX3CL1.

2.8 Neurobehavioral Evaluation

Neurological function was evaluated 72 h after reperfusion by an investigator who was unaware of the experimental grouping. Motor deficits were scored according to the Longa scale (**Supplementary Table 1**), in which higher values represent greater neurological injury. Rats with scores of 2 or 3 were enrolled in the study, while those scoring 0, 1, or 4 were excluded. Sensorimotor function was further evaluated using the Garcia score (**Supplementary Table 2**).

2.9 TTC Staining

At 72 h after reperfusion, rats were deeply anesthetized with an overdose of pentobarbital sodium (150 mg/kg, i.p.) and sacrificed. Brains were rapidly removed and cut into 2 mm coronal sections. Brain sections were stained with 2% TTC (T8877; Sigma-Aldrich) at 37 °C for 20 min, followed by fixation in 4% paraformaldehyde (P6148, Sigma-Aldrich). Infarcted tissue appeared pale, whereas viable tissue was stained red. Infarct volume was quantified using ImageJ software (1.54f, National Institutes of Health, Bethesda, MD, USA) by an investigator blinded to group allocation. To correct for brain edema, relative infarct volume was calculated as follows: [(contralateral hemisphere volume − non-infarcted ipsilateral hemisphere volume) / contralateral hemisphere volume] × 100%.

2.10 Immunofluorescence

Intact brains were postfixed in 4% paraformaldehyde for 24 h, followed by dehydration in 30% sucrose (S0389, Sigma-Aldrich). Briefly, brain sections were rewarmed for 20 min at room temperature (RT). Cells were permeabilized with 0.3% Triton X-100 (T8787, Sigma-Aldrich) for 20 min at 37 °C. Non-specific binding was blocked by treating the sections with goat serum (16210064, Gibco) at 37 °C for 1 h. After washing, the sections were exposed to primary antibodies overnight at 4 °C, including rabbit anti-CYLD (11110-1-AP, Proteintech, Rosemont, IL, USA, 1:100), rabbit anti-SPATA2 (1:100, NBP2-56803, Novus), mouse anti-NeuN (MAB377, Millipore, 1:100, for

neuron labeling), goat anti-Iba1 (NB100-1028SS, Novus, 1:50, for microglia labeling), rabbit anti-HOIP (16289-1-AP, 1:100, Proteintech), mouse anti-cluster of differentiation 86 (CD86, NBP2-25208, 1:100, Novus), and rabbit anti-CD206 (ab64693, 1:100, Abcam, Cambridge, UK). The sections were then reacted with the appropriate fluorescent secondary antibodies for 1 h at 37 °C under light-protected conditions: CoraLite594-conjugated goat anti-rabbit (1:200, SA00013-4, Protein, Wuhan, Hubei, China), CoraLite488-conjugated goat anti-rabbit (1:200, SA00013-2, Protein), CoraLite594-conjugated goat anti-mouse (1:200, SA00013-3, Protein), CoraLite488-conjugated goat anti-mouse (1:200, SA00013-1, Protein), CoraLite594-conjugated donkey anti-rabbit (1:200, SA00013-8, Protein), and fluorescein isothiocyanate (FITC)-conjugated donkey anti-goat (1:200, SA0000334, Protein). The nuclei were stained by using 4′,6-diamidino-2-phenylindole (DAPI; C1005, Beyotime, Shanghai, China). Images were captured on an LSM inverted Confocal Microscope (LSM800, Carl Zeiss Micro-Image, Jena, Germany) and a Nikon A1R Confocal Microscope (Nikon Corporation, Tokyo, Japan). Fields of the peri-ischemic cortex were analyzed in each group.

2.11 RT-qPCR

At 72 h after reperfusion, peri-ischemic cortical tissues were collected, and total RNA was extracted with TRIzol reagent (9108, TaKaRa, Shiga, Japan). Purified RNA was reverse-transcribed into cDNA using the PrimeScript RT reagent kit with gDNA Eraser (RR047A, TaKaRa).

RT-qPCR was performed using a CFX96 Real-Time PCR Detection System (Bio-Rad, Hercules, CA, USA) with SYBR Green chemistry (SYBR Premix Ex Taq II, RR820A; Takara Bio, Kusatsu, Shiga, Japan). The primer sequences are reported in (Table 1). Melting-curve analysis was used to verify primer–target specificity for each sample. The data were normalized to the gene expression of glyceraldehyde-3-phosphate dehydrogenase (GAPDH). Relative mRNA expression was calculated using the $2^{-\triangle\triangle Ct}$ method.

Table 1. Primer sequences for RT-qPCR.

Name	Sequence
SPATA2-F	CCCTCAAAGGCCTCACTGAG
SPATA2-R	ACATGGTCAGCAATGAGGGG
GAPDH-F	ATGATTCTACCCACGGCAAG
GAPDH-R	CTGGAAGATGGTGATGGGTT

RT-qPCR, real-time quantitative polymerase chain reaction; SPATA2, spermatogenesis-associated protein 2; GAPDH, glyceraldehyde-3-phosphate dehydrogenase.

2.12 Western Blot Analysis

Tissues were homogenized in radioimmunoprecipitation assay (RIPA) lysis buffer (Beyotime, P0013B) supplemented with phenylmethylsulfonyl fluoride (PMSF, ST505, Beyotime). Supernatants from peri-ischemic samples were centrifuged at 12,000 rpm for 15 min at 4 °C. For each sample, 30 µg of protein was separated on 8–12% sodium dodecyl sulfate–polyacrylamide gel electrophoresis (SDS-PAGE, P0012A, Beyotime) gels and then electrotransferred to 0.46/0.22 µm polyvinylidene fluoride (PVDF) membranes (0.2 µm pore size; ISEQ00010, Millipore, Burlington, MA, USA). Membranes were first blocked for 1 h and then exposed to the indicated primary antibodies overnight at 4 °C: anti-CYLD rabbit (1:1500, 11110-1-AP, Proteintech), anti-CX3CL1 rabbit (ab25093, Abcam, 1:1000), mouse anti-GAPDH (60004-1-Ig, Proteintech, 1:5000), anti-CX3CR1 mouse (sc-30030, Santa Cruz, 1:1000, Dallas, TX, USA), anti-SPATA2 rabbit (NBP2-56803, Novus, 1:1000) and anti-HOIP rabbit (16289-1-AP, Proteintech, 1:1500). The membranes were subsequently reacted with horseradish peroxidase-conjugated secondary antibodies for 1 h at room temperature, including goat anti-rabbit (SA00001-2, Proteintech, 1:3000) and goat anti-mouse (SA00001-1, Proteintech, 1:3000). Immunoreactive bands were visualized and recorded using a gel imaging system (Fusion FX7 Spectra, Vilber Lourmat, Collégien, France). Band intensity quantification was performed using the corresponding FUSION-CAPT analysis software (version 15.12; Vilber Lourmat).

2.13 Co-Immunoprecipitation

Lysates from the Transwell neuron-microglia co-culture system were homogenized in immunoprecipitation (IP) lysis buffer (87787, Thermo Fisher Scientific) to extract total proteins. For the immunoprecipitation step, equal quantities of protein from the supernatants were mixed with antibodies against HOIP (16289-1-AP, Proteintech) or CX3CR1 (sc-30030, Santa Cruz), or with control immunoglobulin G (IgG, A7016, Beyotime), and maintained overnight at 4 °C. Next, 20 µL of Protein A/G agarose beads (20241, Thermo Fisher Scientific) was added to each sample, followed by rotation at 4 °C for 4–6 h. After washing with lysis buffer (87787, Thermo Fisher Scientific), the beads were resuspended in 40 µL of SDS loading buffer and processed for Western blotting.

2.14 ELISA

Culture supernatants were collected from Transwell neuron–microglia co-cultures after the indicated treatments and centrifuged to remove cell debris. Concentrations of IL-1β (E-EL-R0012, Elabscience), IL-6 (E-EL-R0015, Elabscience), TNF-α (E-EL-R2856, Elabscience), IL-10 (E-EL-R0016, Elabscience), and CX3CL1 (E-EL-R0385, Elabscience) were quantified with commercially available ELISA kits following the protocols supplied by the manu-

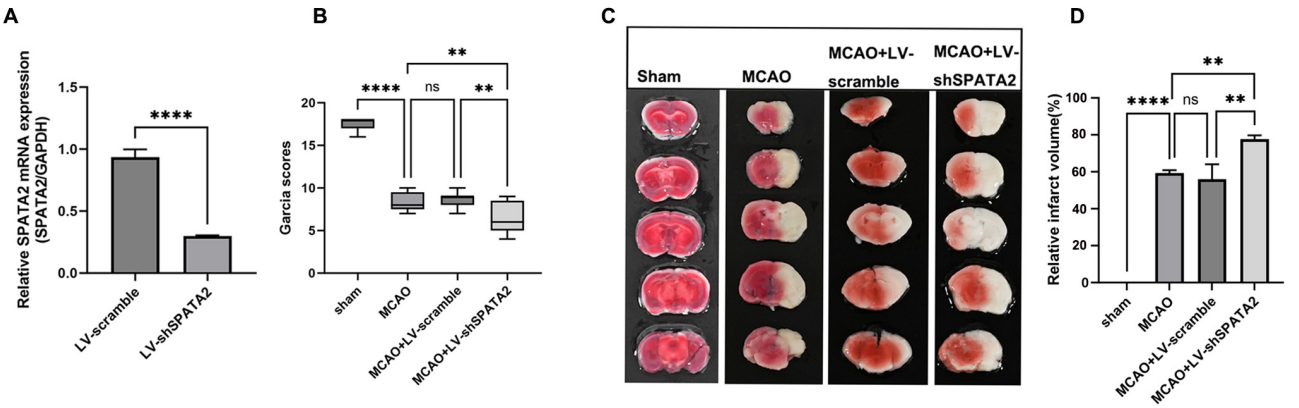


Fig. 1. SPATA2 knockdown worsens neurological performance and increases infarct volume in a rat MCAO model. (A) SPATA2 mRNA levels in rats receiving LV-scramble or LV-shSPATA2 were detected using RT-qPCR (n = 3) and normalized to GAPDH. (B) Neurological function was assessed using the Garcia score in four experimental groups: sham, MCAO, MCAO + LV-scramble, and MCAO + LV-shSPATA2. Higher scores indicate better neurological function. (C) Representative TTC-stained brain sections from rats in each group. (D) Relative cerebral infarct volume was quantified after MCAO in the indicated groups. Infarct volume is expressed as a percentage of the contralateral hemisphere. Data are presented as mean ± SEM; n = 3 rats per group. Statistical comparisons were performed using one-way ANOVA followed by Tukey's multiple comparisons test. $^{**}p < 0.01$ and $^{****}p < 0.0001$; ns, not significant. MCAO, middle cerebral artery occlusion; LV-shSPATA2, lentiviral vectors carrying either SPATA2-specific shRNA; TTC, 2,3,5-triphenyltetrazolium chloride; SEM, standard error of the mean; ANOVA, analysis of variance.

facturers. CX3CL1 measured by ELISA was operationally defined as soluble CX3CL1 released into the culture supernatant. This assay did not measure membrane-bound CX3CL1 or total cellular CX3CL1.

2.15 Primary Cortical Neurons Electroporation

Before plating, primary cortical neurons were subjected to electroporation with Gene Pulser Xcell Electroporation System (1652660, Bio-Rad) following the manufacturer's protocol. For SPATA2 knockdown, neurons were transfected with SPATA2-specific siRNAs or siRNA negative control. For SPATA2 overexpression, neurons were electroporated with pcDNA3.1-SPATA2 or empty pcDNA3.1 vector. For rescue experiments, CYLD-specific siRNA or siRNA negative control was introduced into SPATA2-overexpressing neurons by electroporation.

Following electroporation, neurons were plated on poly-L-lysine-coated plates or coverslips and maintained in Neurobasal medium containing B27 and L-glutamine. Following neuronal gene manipulation, primary microglia were added to establish the Transwell neuron-microglia co-culture system. Microglia were not subjected to electroporation.

2.16 Statistical Analysis

All statistical analyses were performed using GraphPad Prism 8.0 (GraphPad Software, San Diego, CA, USA). Data are presented as mean ± standard error of the mean (SEM). The number of independent biological replicates is 3. For *in vivo* experiments, each rat was considered one independent biological replicate. For primary cell culture and Transwell co-culture experiments, independent biological replicates were defined as independent cell preparations. Values obtained from technical replicates or from multiple microscopic fields within the same animal or culture preparation were first averaged, and only the corresponding biological replicate was entered into the statistical analysis. Biological replicates were used as the unit of statistical analysis for all experiments.

Differences between two groups were analyzed using an unpaired two-tailed Student's *t*-test. When more than two groups were compared, one-way analysis of variance (ANOVA) was performed, followed by Tukey's multiple comparisons test. For experiments with two independent factors, such as transfection condition and OGD/R exposure, data were evaluated by two-way ANOVA with Sidak's multiple comparisons test. A value of $p < 0.05$ was considered statistically significant.

3. Results

3.1 SPATA2 Knockdown Exacerbates Infarct Burden and Worsens Neurological Deficits After MCAO

To assess the contribution of SPATA2 to ischemic injury, LV-shSPATA2 was used to reduce SPATA2 expression in the rat brain. RT-qPCR confirmed that SPATA2 mRNA expression was significantly lower in LV-shSPATA2-treated rats than in LV-scramble controls (Fig. 1A). We next evaluated the effects of SPATA2 knockdown on stroke outcomes in an MCAO model. The Garcia neurological score was markedly lower in the MCAO + LV-shSPATA2 group than in the MCAO + LV-scramble group,

suggesting that SPATA2 knockdown aggravated neurological deficits (Fig. 1B). Consistently, TTC staining further showed a larger infarct volume in the MCAO + LV-shSPATA2 group than in the MCAO + LV-scramble group (Fig. 1C,D). These findings indicate that SPATA2 silencing exacerbates neurological deficits and ischemic brain injury following MCAO.

3.2 SPATA2 Knockdown Enhances Pro-Imflammatory Microglial Marker Expression In Vivo

Separate double-immunofluorescence staining of SPATA2 with NeuN, Iba1, or glial fibrillary acidic protein (GFAP) was performed to examine the cellular localization of SPATA2 in the peri-ischemic cortex. Representative images showed that SPATA2 immunoreactivity predominantly overlapped with NeuN-positive neurons, whereas

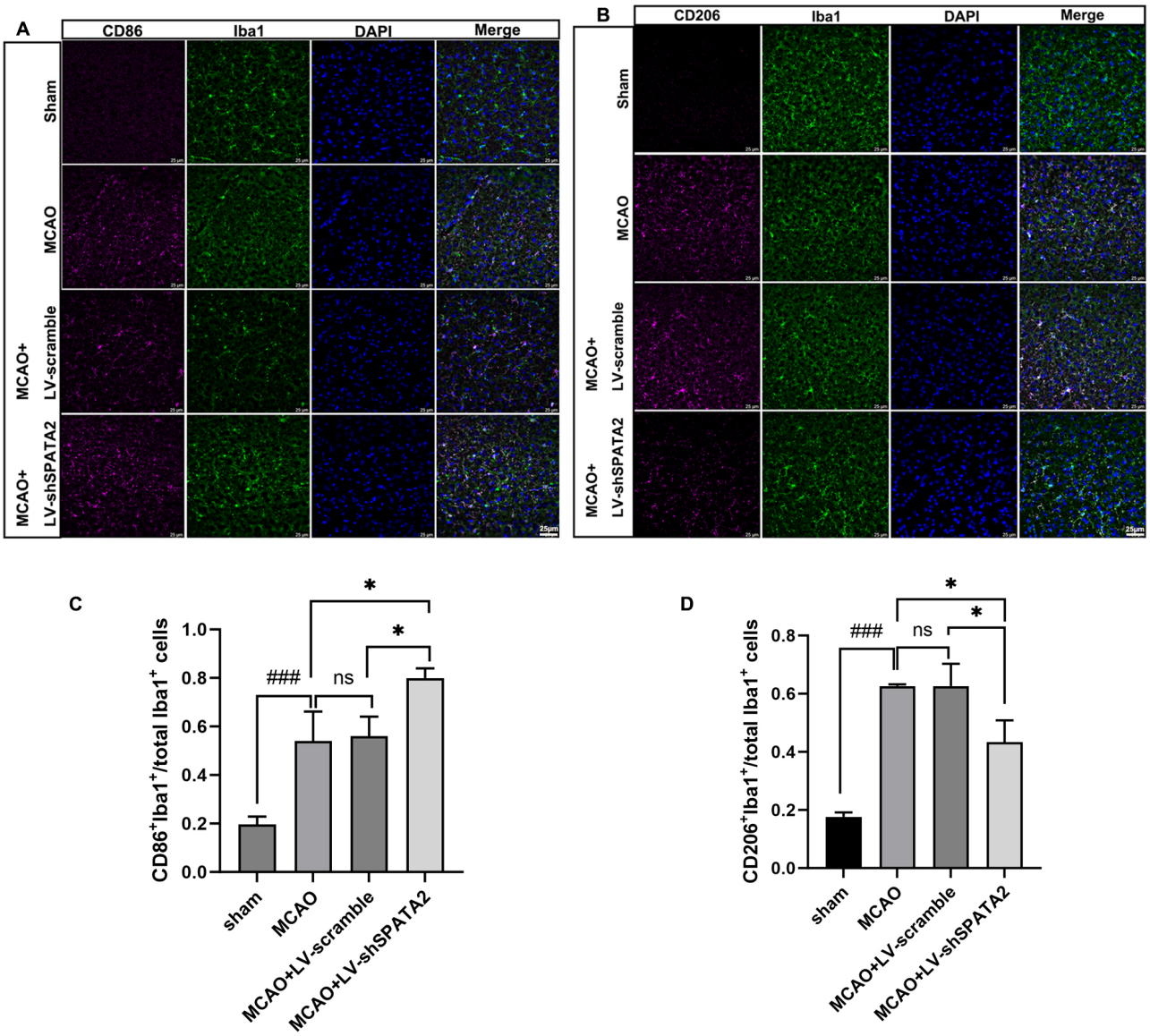


Fig. 2. SPATA2 knockdown alters selected microglial inflammatory markers in the peri-ischemic cortex after MCAO. (A) Immunofluorescence staining of brain sections from sham, MCAO, MCAO + LV-scramble, and MCAO + LV-shSPATA2 groups. Sections were stained for CD86, Iba1, and DAPI. Scale bar = 25 μm. (B) Representative images of CD206, Iba1, and DAPI staining are shown for the corresponding experimental groups. (C) Quantitative analysis of the proportion of Iba1+/CD86+ cells relative to the total number of Iba1-positive cells in the peri-ischemic cortex across groups. (D) Quantitative analysis of the proportion of Iba1+/CD206+ cells relative to the total number of Iba1-positive cells in the peri-ischemic cortex across groups. Data are presented as mean ± SEM; n = 3 rats per group. Statistical comparisons were performed using one-way ANOVA followed by Tukey's multiple comparisons test. $^{*}p < 0.05$ and $^{###}p < 0.001$; ns, not significant. Iba1, ionized calcium-binding adapter molecule 1; DAPI, 4′,6-diamidino-2-phenylindole; CD86, cluster of differentiation 86.

relatively limited overlap was observed with Iba1-positive microglia or GFAP-positive astrocytes (**Supplementary Fig. 1**). We next examined microglial activation-related markers in ischemic brain tissue to evaluate how SPATA2 loss affected the inflammatory profile of microglia. Compared with the Sham group, MCAO significantly increased the proportions of both Iba1+/CD86+ and Iba1+/CD206+ cells among total Iba1-positive cells, indicating that MCAO induced marked changes in microglial inflammatory marker profiles in the peri-ischemic cortex (Fig. 2A–D). No significant differences were observed between the MCAO and MCAO + LV-scramble groups, suggesting that LV-scramble administration did not substantially affect these marker profiles (Fig. 2C,D). Immunofluorescence staining revealed a higher proportion of Iba1+/CD86+ cells among total Iba1-positive cells in the MCAO + LV-shSPATA2 group than in the MCAO + LV-scramble group (Fig. 2A,C). In contrast, the proportion of Iba1+/CD206+ cells among total Iba1-positive cells was lower in the MCAO + LV-shSPATA2 group than in the MCAO + LV-scramble group (Fig. 2B,D). Overall, these results show that MCAO induced significant microglial inflammatory marker changes, whereas SPATA2 knockdown further shifted these changes toward an increased proportion of Iba1+/CD86+ cells and decreased proportion of Iba1+/CD206+ cells in the peri-ischemic cortex after MCAO.

3.3 SPATA2 Regulates Microglial Inflammatory Responses In Vitro

To manipulate SPATA2 expression in primary cortical neurons, cells were electroporated with si-SPATA2 (siRNA 1, siRNA 2, and siRNA 3) and pcDNA3.1-SPATA2 to establish SPATA2 knockdown and overexpression models. RT-qPCR analysis showed that siRNA1 achieved higher knockdown efficiency than siRNA2 and siRNA3 (Fig. 3A). In addition, SPATA2 mRNA expression was significantly higher in the pcDNA3.1-SPATA2 group than in the pcDNA3.1 negative control group (Fig. 3B). Western blotting further confirmed the corresponding decrease or increase in SPATA2 protein expression in neurons (Fig. 3C,D).

To assess neuron-to-microglia regulation, we constructed a Transwell co-culture model using SPATA2-manipulated primary neurons and microglia. SPATA2 was knocked down or overexpressed in primary cortical neurons by electroporation before the addition of microglia to the Transwell inserts (Fig. 4A). This configuration allowed communication between neurons and microglia predominantly through soluble paracrine factors without direct cell–cell contact.

Immunofluorescence staining showed that neuronal SPATA2 knockdown increased CD86 expression in Iba1-positive microglia, whereas SPATA2 overexpression reduced CD86 expression (Fig. 4B). Morphologically, microglia in the SPATA2 knockdown condition exhibited a more amoeboid appearance, whereas SPATA2 overexpression attenuated these changes (Fig. 4A). ELISA assays showed that supernatants from the SPATA2 knockdown condition contained higher amounts of IL-1β, IL-6, and TNF-α but lower IL-10 levels. Conversely, overexpression of SPATA2 produced the opposite cytokine pattern, with reduced IL-1β, IL-6, and TNF-α and elevated IL-10 (Fig. 4C–F). These results suggest that neuron-derived SPATA2 attenuates microglial pro-inflammatory responses in the Transwell co-culture system.

3.4 SPATA2 Modulates CYLD Related NF-κB/CX3CR1 Signaling

To explore how SPATA2 affects inflammatory signaling, we analyzed CYLD, NF-κB, and CX3CR1-related proteins in Transwell neuron–microglia co-culture model. Western blotting revealed opposite changes after SPATA2 loss and gain of function: neuronal SPATA2 knockdown lowered CYLD expression but elevated NF-κB p65 levels (Fig. 5A–C, the original uncropped Western blot images are available in the **Supplementary Material**), whereas SPATA2 overexpression increased CYLD and reduced NF-κB p65. These results link SPATA2 expression to changes in CYLD abundance and NF-κB-related inflammatory signaling.

Given the reported adaptor role of SPATA2 in recruiting CYLD to HOIP/LUBAC-containing complexes, we next used co-immunoprecipitation (Co-IP) assays to assess protein associations in the neuron–microglia co-culture system. Co-IP using an anti-HOIP antibody revealed detectable CYLD-HOIP association, which was enhanced by SPATA2 overexpression and reduced by SPATA2 knockdown (Fig. 5D, the original uncropped Western blot images are available in the **Supplementary Material**). In addition, Co-IP using an anti-CX3CR1 antibody indicated that SPATA2 manipulation altered CX3CL1/CX3CR1-associated protein complexes in cell lysates (Fig. 5E, the original uncropped Western blot images are available in the **Supplementary Material**). Because these assays were performed using lysates from the Transwell co-culture system, they do not identify the precise cellular source of each protein and do not directly measure ligand-receptor binding on the intact cell surface.

To determine whether CYLD contributes to SPATA2-mediated regulation of inflammatory signaling, CYLD was knocked down in SPATA2-overexpressing neurons. Western blot analysis confirmed that SPATA2 overexpression increased CYLD expression and reduced NF-κB p65 expression (Fig. 5F–I, the original uncropped Western blot images are available in the **Supplementary Material**). CYLD silencing reduced CYLD protein abundance and partially reversed the suppressive effect of SPATA2 overexpression on NF-κB p65 expression. In parallel, ELISA showed that CYLD silencing partially reversed the reduction in soluble

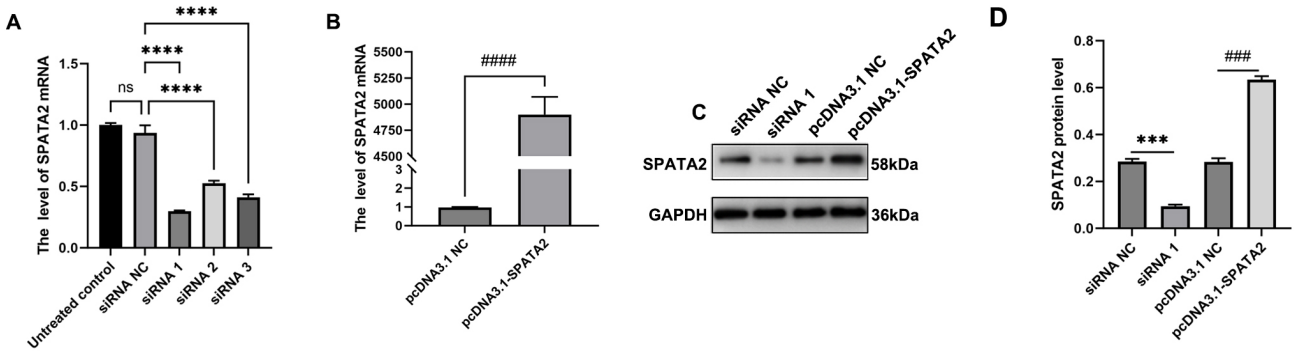


Fig. 3. Efficient knockdown and overexpression of SPATA2 in primary neurons. (A) Relative SPATA2 mRNA expression in untreated control neurons, siRNA NC-transfected cells, and neurons transfected with SPATA2 siRNAs (siRNA1, siRNA2, and siRNA3), as determined by RT-qPCR and normalized to GAPDH. (B) Relative mRNA expression of SPATA2 in cells transfected with pcDNA3.1 NC or pcDNA3.1-SPATA2 was measured by RT-qPCR. SPATA2 expression was normalized to GAPDH. (C) Representative Western blot images showing SPATA2 protein levels in SPATA2 knockdown (siRNA NC, siRNA 1) and SPATA2 overexpression (pcDNA3.1 NC, pcDNA3.1-SPATA2) cells. GAPDH was used as a loading control. (D) Quantification of SPATA2 protein levels from Western blot experiments. Protein levels were normalized to GAPDH. Data are presented as mean ± SEM. n = 3 independent cell preparations per group. Statistical comparisons were performed using one-way ANOVA followed by Tukey's multiple comparisons test for (A) and an unpaired two-tailed Student's *t*-test for the two-group comparisons in (B,D). $^{***}p < 0.001$ and $^{****}p < 0.0001$ vs. siRNA NC group; $^{\#\#\#}p < 0.001$ and $^{\#\#\#\#}p < 0.0001$ vs. pcDNA3.1 NC group; ns, not significant. NC, negative control.

CX3CL1 release induced by SPATA2 overexpression (Fig. 5J). Together, these results indicate that CYLD contributes to SPATA2-associated regulation of NF-κB p65 expression and soluble CX3CL1 release, although they do not establish CYLD as the sole mediator of this process.

3.5 SPATA2 Alters Soluble CX3CL1 Release Under OGD/R Conditions in Transwell Co-Culture

To further examine SPATA2-associated responses under ischemia-like conditions *in vitro*, the Transwell neuron–microglia co-culture system was subjected to OGD/R. Western blotting revealed lower SPATA2 and CYLD protein expression after OGD/R exposure than under the corresponding normoxic control conditions (Fig. 6A–C, the original uncropped Western blot images are available in the **Supplementary Material**). Under OGD/R conditions, SPATA2 knockdown caused an additional reduction in SPATA2 expression but was accompanied by a relative decrease in CYLD expression compared with the corresponding siRNA NC group. SPATA2 overexpression restored SPATA2 expression and was accompanied by changes in CYLD expression under OGD/R conditions. These observations indicate that the relationship between SPATA2 manipulation and CYLD abundance differs between normoxic and OGD/R conditions.

We next measured soluble CX3CL1 levels in the co-culture supernatants by ELISA. OGD/R significantly increased soluble CX3CL1 release. SPATA2 knockdown further enhanced the OGD/R-induced increase in soluble CX3CL1, whereas SPATA2 overexpression attenuated this increase (Fig. 6D). Taken together, these data show that SPATA2 is associated with changes in soluble CX3CL1 release in the Transwell neuron–microglia co-culture system exposed to OGD/R.

4. Discussion

As the resident innate immune cells in the central nervous system, microglia are key participants in the inflammatory cascade triggered by ischemic stroke [32]. Their effects are context dependent: microglia may support debris removal and tissue remodeling, whereas excessive activation can worsen inflammation by promoting the production of pro-inflammatory mediators [33,34,35]. In this study, loss of SPATA2 worsened neurological outcomes and enlarged the infarct area following middle cerebral artery occlusion/reperfusion (MCAO/R). At the same time, SPATA2 deficiency was accompanied by a higher proportion of Iba1+/CD86+ cells and a lower proportion of Iba1+/CD206+ cells in the peri-ischemic cortex. These results link SPATA2 to the control of post-ischemic inflammation and to changes in selected microglial inflammatory marker profiles.

After ischemic injury, microglial activation encompasses diverse cellular states that are not adequately captured by a binary M1/M2 framework [32]. CD86, CD206, morphology, and cytokine measurements do not comprehensively define the heterogeneous microglial states that emerge after ischemic injury. However, we recognize that these markers do not define complete microglial state transitions. Accordingly, the revised manuscript describes these observations more conservatively as alterations in selected pro-inflammatory and anti-inflammatory/reparative markers. The increase in the proportion of Iba1+/CD86+

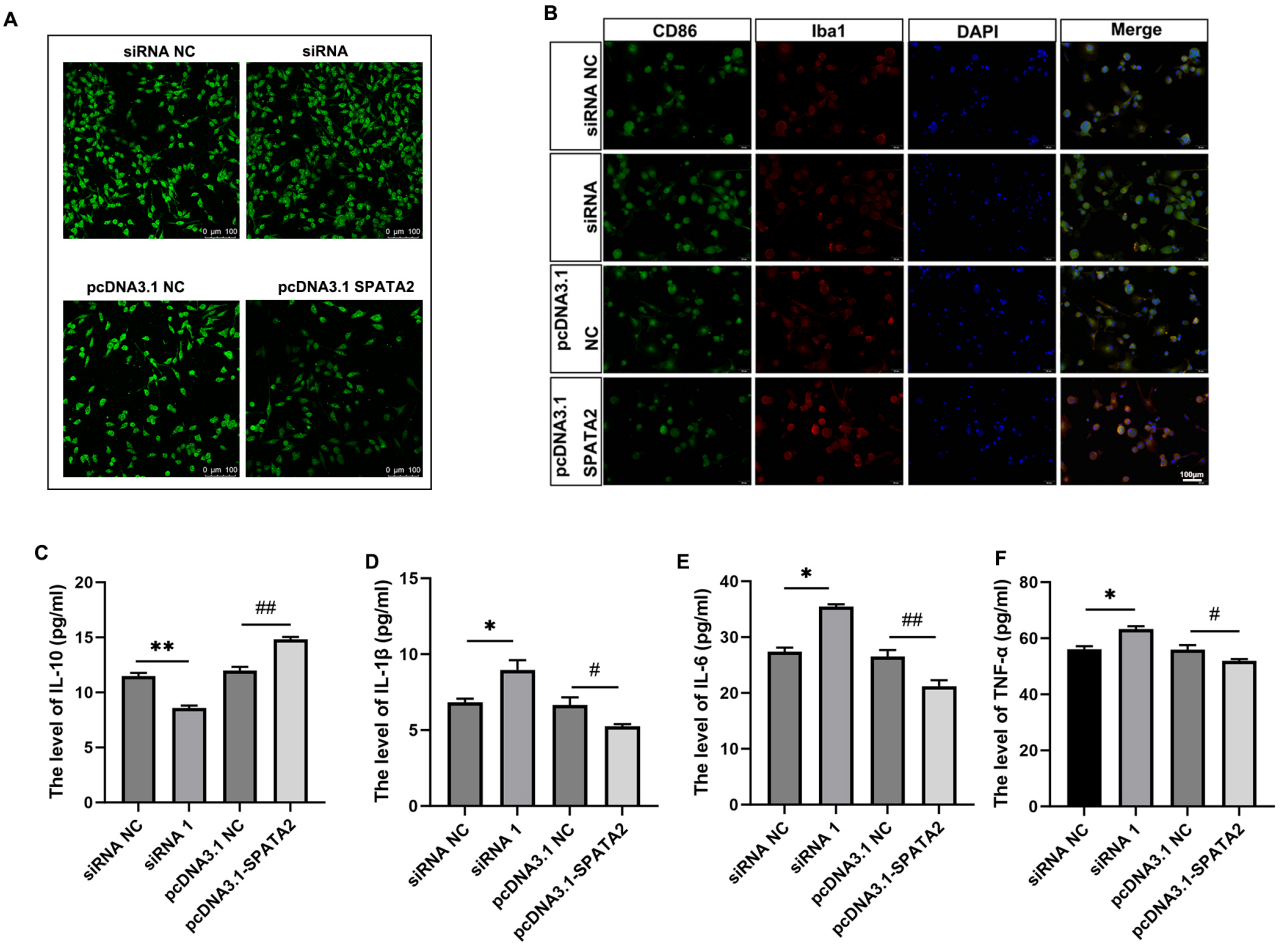


Fig. 4. SPATA2 modulates microglial inflammatory marker profiles and inflammatory cytokine secretion *in vitro*. (A) Representative morphology of microglia following Transwell co-cultural system. Scale bar = 100 μm. (B) IF staining of microglia. Cells were co-stained for CD86 (a pro-inflammatory-associated microglial marker, green), Iba1 (pan-microglial marker, red), and DAPI (nuclear, blue). Merged images show the co-localization of CD86 and Iba1. Scale bar = 100 μm. (C–F) ELISA-based quantification of IL-10 (C), IL-1β (D), IL-6 (E), and TNF-α (F) levels in culture supernatants collected from the indicated groups. Data are presented as mean ± SEM. n = 3 independent cell preparations per group. Statistical comparisons were performed using one-way ANOVA followed by Tukey's multiple comparisons test. $^{*}p < 0.05$ and $^{**}p < 0.01$ vs. siRNA NC group; $^{\#}p < 0.05$ and $^{\#\#}p < 0.01$ vs. pcDNA3.1 NC group. IF, immunofluorescence; ELISA, enzyme-linked immunosorbent assay; IL-10, interleukin-10; TNF-α, tumor necrosis factor alpha.

cells after SPATA2 knockdown is consistent with a stronger pro-inflammatory marker pattern, whereas the reduction in the proportion of Iba1+/CD206+ cells indicates attenuation of a selected anti-inflammatory/reparative feature. When considered alongside the cytokine results from the Transwell co-culture model, these findings indicate that SPATA2 affects microglial inflammatory responses rather than establishing a complete transition between predefined M1-like and M2-like states. Recent experimental studies have similarly linked modulation of microglial inflammatory responses and NLRP3-related signaling to reduced ischemic brain injury [36].

Neuron–microglia communication is an important contributor to neuroinflammation after ischemic injury [37]. In this study, we used a Transwell neuron–microglia co-culture model to examine whether neuron-derived SPATA2 affects microglial inflammatory responses. Because neurons and microglia were separated by the Transwell membrane, this model mainly reflects paracrine communication rather than direct cell–cell contact. Within this co-culture setting, loss of neuronal SPATA2 increased microglial CD86 staining and promoted the secretion of IL-1β, IL-6, and TNF-α. In contrast, neuronal SPATA2 overexpression attenuated these pro-inflammatory changes and elevated IL-10 levels. These observations indicate that neuronal SPATA2 may influence inflammatory communication between neurons and microglia through soluble mediators. Nevertheless, this *in vitro* system cannot capture the full complexity of the ischemic brain microenvironment, which involves dynamic interactions among neurons, microglia, astrocytes, endothelial cells, infiltrating immune cells, and extracellular matrix components [38].

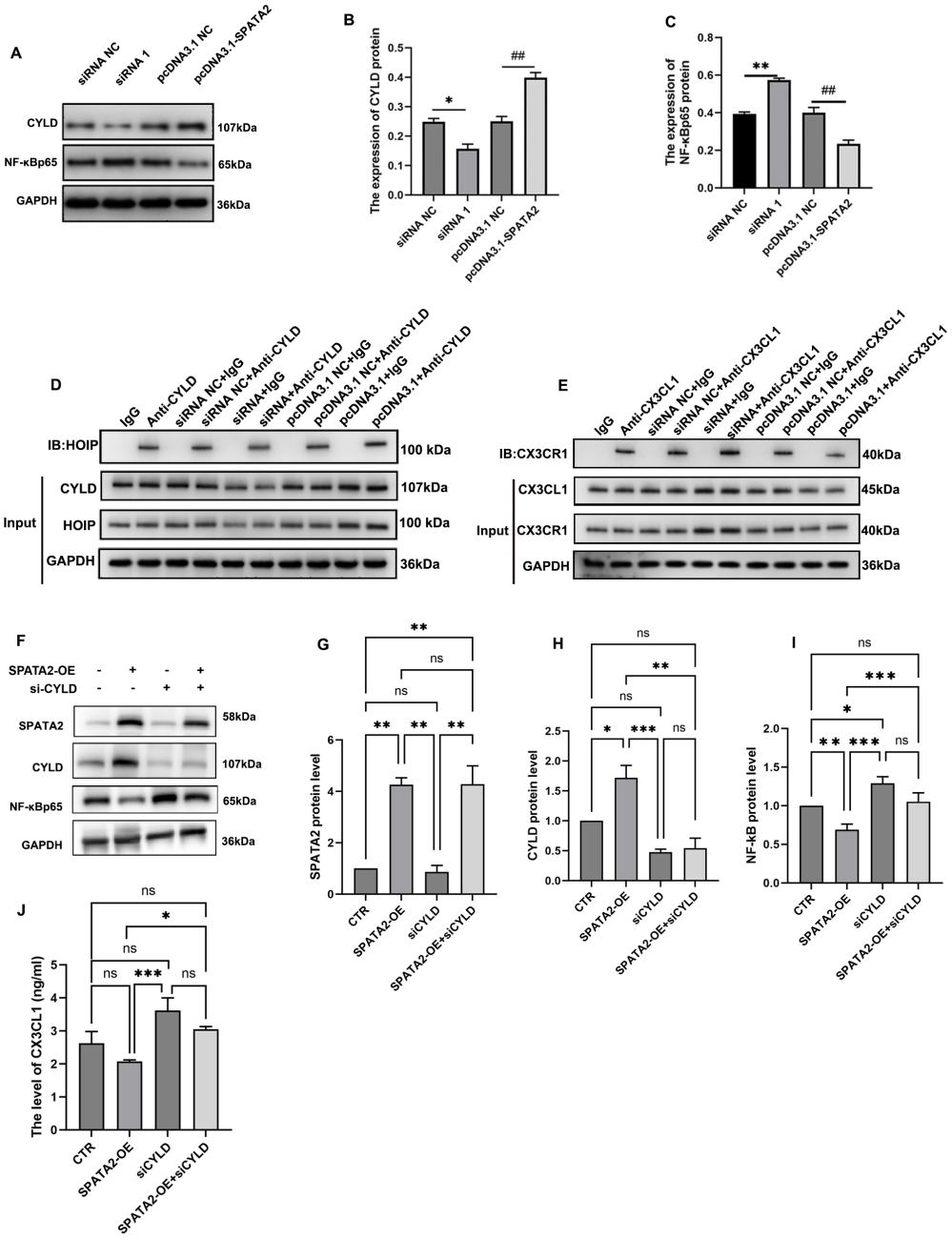


Fig. 5. SPATA2 modulates CYLD-associated inflammatory signaling *in vitro*. (A) Representative Western blot images showing SPATA2, CYLD, and NF-κB p65 protein expression after SPATA2 knockdown or overexpression in the Transwell neuron–microglia co-culture system. GAPDH was used as the loading control. (B,C) Quantification of CYLD and NF-κB p65 protein levels normalized to GAPDH. (D) Co-IP using lysates from the Transwell co-culture system immunoprecipitated with an anti-HOIP antibody or control IgG, followed by immunoblotting for CYLD and HOIP. (E) Co-IP using an anti-CX3CR1 antibody or control IgG, followed by immunoblotting for CX3CL1 and CX3CR1. These Co-IP results indicate detectable protein associations in co-culture lysates and do not directly demonstrate ligand–receptor binding at the intact cell surface. (F) Representative Western blot images showing SPATA2, CYLD, and NF-κB p65 expression in the control, SPATA2-OE, siCYLD, and SPATA2-OE + siCYLD groups. (G–I) Quantification of SPATA2, CYLD, and NF-κB p65 protein levels normalized to GAPDH. (J) ELISA-based quantification of soluble CX3CL1 in culture supernatants from the control, SPATA2-OE, siCYLD, and SPATA2-OE + siCYLD groups. Data are presented as mean ± SEM; n = 3 independent cell preparations per group for quantitative experiments. Statistical comparisons were performed using one-way ANOVA followed by Tukey's multiple comparisons test. $^{*}p < 0.05$, $^{**}p < 0.01$ and $^{***}p < 0.001$; $^{\#\#}p < 0.01$; ns, not significant. CYLD, cylindromatosis; NF-κB, nuclear factor-κB; HOIP, heme-oxidized IRP2 ubiquitin ligase1-like interacting protein; IgG, immunoglobulin G; CX3CR1, CX3C chemokine receptor 1; CX3CL1, C-X-C motif 3 chemokine ligand 1; Co-IP, co-immunoprecipitation; OE, overexpression.

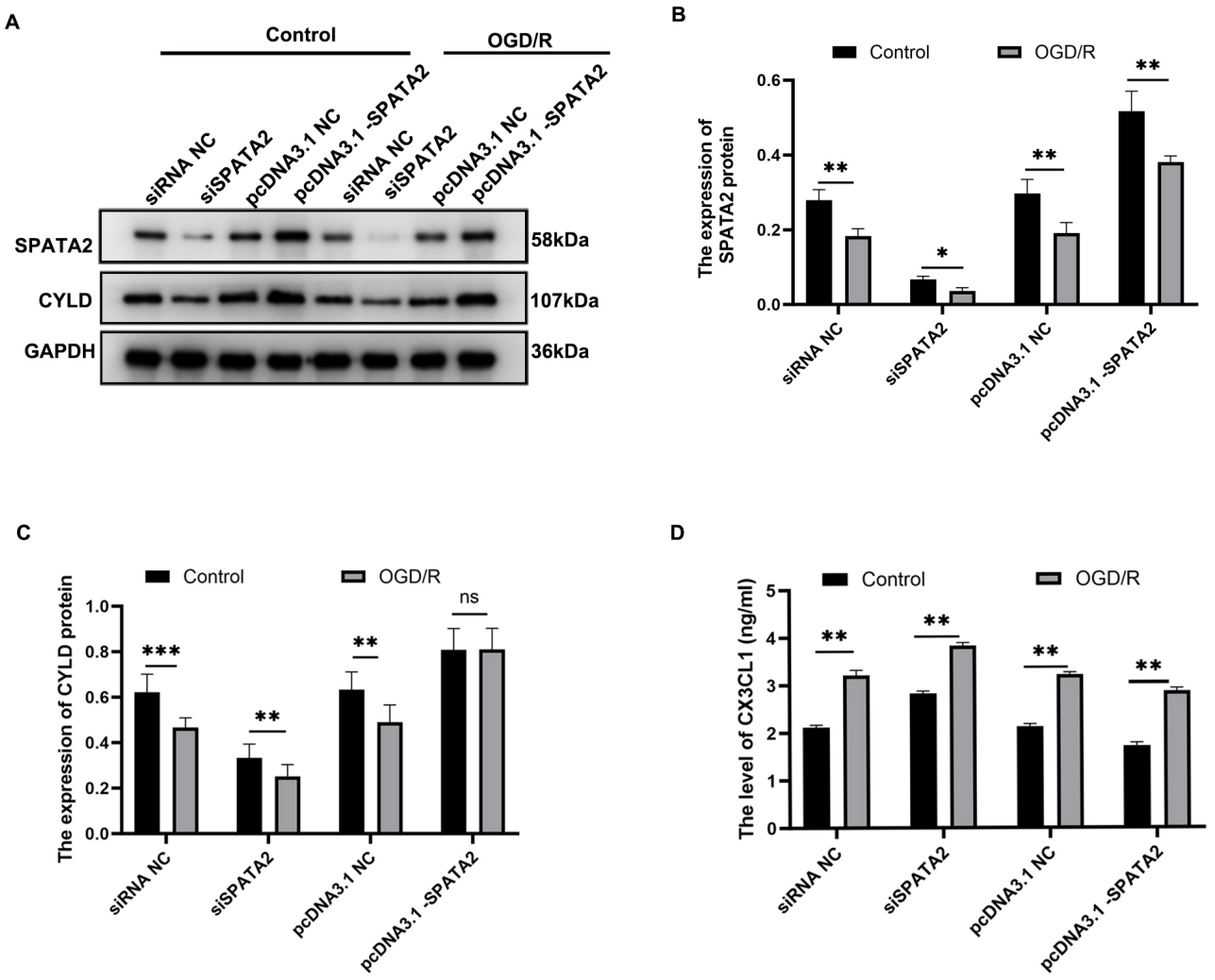


Fig. 6. SPATA2 modulates CYLD expression and soluble CX3CL1 release under OGD/R conditions *in vitro*. (A) Representative Western blot images showing SPATA2 and CYLD expression in neuronal lysates collected from the lower chamber of the Transwell co-culture system under normoxic or OGD/R conditions. Neurons were electroporated with siRNA NC, siSPATA2, pcDNA3.1 NC, or pcDNA3.1-SPATA2 before co-culture. (B,C) Quantification of SPATA2 and CYLD protein levels normalized to GAPDH. (D) ELISA-based quantification of soluble CX3CL1 in co-culture supernatants collected from the indicated groups under normoxic or OGD/R conditions. Data are presented as mean ± SEM; n = 3 independent cell preparations per group. Data were analyzed using two-way ANOVA followed by Sidak's multiple comparisons test. $^{*}p < 0.05$, $^{**}p < 0.01$ and $^{***}p < 0.001$ vs. control group; ns, not significant. OGD/R, oxygen-glucose deprivation/reperfusion.

An important issue raised by the reviewers concerns the cell-type specificity of SPATA2 *in vivo*. In the present study, the *in vivo* knockdown was performed by intracerebroventricular lentiviral delivery using a broad promoter, and the virus did not contain a fluorescent reporter. Therefore, the *in vivo* manipulation cannot be considered strictly neuron-specific. To better characterize SPATA2 localization, we added separate double-immunofluorescence staining experiments for SPATA2/NeuN, SPATA2/Iba1, and SPATA2/GFAP. Representative images showed that SPATA2 immunoreactivity predominantly overlapped with NeuN-positive neurons and showed relatively limited overlap with Iba1-positive microglia or GFAP-positive astrocytes in the peri-ischemic cortex. Because quantitative colocalization analysis was not performed, these images provide qualitative support for neuron-enriched SPATA2 localization but do not establish neuron-specific expression. Potential contributions from non-neuronal cells therefore cannot be fully excluded in the *in vivo* experiments. Accordingly, the *in vivo* data indicate that reducing SPATA2 expression in the peri-ischemic cortex worsens inflammatory injury, whereas the Transwell experiments more specifically implicate neuron-derived SPATA2 in the regulation of microglial inflammatory responses.

CYLD, a deubiquitinase, has been widely recognized as an anti-inflammatory regulator, in part because it re-

strains NF-κB signaling [39]. SPATA2 has been reported to act as an adaptor that links CYLD to HOIP/LUBAC-containing signaling complexes [20]. Here, altering SPATA2 expression changed the abundance of CYLD and NF-κB p65, and the Co-IP results were consistent with an association between CYLD and HOIP. Notably, the additional CYLD loss-of-function experiment demonstrated that CYLD silencing weakened, but did not completely abolish, the suppressive effects of SPATA2 overexpression on NF-κB p65 expression and soluble CX3CL1 release. These findings strengthen the evidence that CYLD contributes to SPATA2-associated suppression of inflammatory signaling. However, the data do not establish every step of the SPATA2–CYLD–HOIP pathway as a direct causal sequence *in vivo*. Therefore, we interpret CYLD as an important contributor to, rather than the sole mediator of, SPATA2-regulated inflammatory responses.

The relationship between SPATA2, CYLD, and CX3CL1/CX3CR1-related signaling also requires cautious interpretation. CX3CL1 is a key neuron–microglia communication molecule and may exist in both membrane-bound and soluble forms [15,40]. In our ELISA experiments, CX3CL1 refers specifically to soluble CX3CL1 released into the culture supernatant of the Transwell co-culture system. By comparison, the Co-IP assay using lysates from the Transwell co-culture system detected CX3CL1/CX3CR1-associated protein complexes. Because the lysates contained material from the co-culture system, this assay does not identify the precise cellular source of each protein. Moreover, Co-IP cannot directly assess ligand–receptor engagement on the intact cell surface. Accordingly, the present results are best interpreted as evidence that SPATA2 is associated with changes in CX3CL1/CX3CR1-related pathway activity, without demonstrating direct inhibition of CX3CL1–CX3CR1 binding at the cell surface.

The OGD/R experiments further suggest that SPATA2 influences soluble CX3CL1 release under ischemia-like inflammatory stress. In the Transwell co-culture supernatant, soluble CX3CL1 release was elevated after OGD/R exposure. This response was further amplified when SPATA2 was knocked down, whereas SPATA2 overexpression reduced the OGD/R-induced increase. Interestingly, CYLD regulation under OGD/R appeared context dependent. Although OGD/R reduced CYLD expression compared with the corresponding normoxic controls, SPATA2 knockdown produced a relative increase in CYLD under the same oxygenation condition. This apparent discrepancy may reflect a stress-associated compensatory response in the OGD/R setting rather than enhanced CYLD functional recruitment. Because SPATA2 is required for efficient CYLD association with HOIP/LUBAC-containing complexes, total CYLD abundance alone may not fully reflect CYLD functional activity [20]. The CYLD knockdown experiment further indicates that CYLD is functionally involved in SPATA2-dependent regulation of NF-κB p65 expression and soluble CX3CL1 release. Nevertheless, additional work is needed to clarify how ischemic stress affects CYLD abundance, subcellular localization, and recruitment.

On the basis of these observations, we suggest that SPATA2 may limit post-ischemic inflammatory injury through effects on CYLD-related inflammatory signaling and CX3CL1/CX3CR1-related neuron–microglia communication. Within this framework, SPATA2 may facilitate CYLD-linked control of NF-κB-related signaling and decrease soluble CX3CL1 release during OGD/R, which may contribute to the restraint of selected pro-inflammatory microglial responses. However, this model should be considered hypothesis-generating rather than fully proven. Further investigation using neuron-specific viral promoters, conditional genetic models, CX3CR1 blockade, CX3CL1 neutralization, HOIP/LUBAC inhibition, and single-cell or spatial transcriptomic approaches will be necessary to resolve the causal sequence and cell-type-specific mechanisms underlying this pathway.

5. Limitation

Several limitations of this study should be acknowledged. First, the intracerebroventricular lentiviral vector used *in vivo* was driven by a broad promoter and lacked a fluorescent reporter; therefore, the manipulation was not neuron-specific, and contributions from non-neuronal cells cannot be excluded. Second, microglial inflammatory responses were evaluated using selected markers, including CD86, CD206, morphology, and a limited cytokine panel. These measurements do not provide comprehensive characterization of the heterogeneous microglial states present after ischemic injury. Third, the Transwell system reflects soluble paracrine communication without direct neuron–microglia contact and does not reproduce the full cellular complexity of the ischemic brain. Fourth, CX3CL1 was operationally assessed differently across assays: ELISA measured soluble CX3CL1 in culture supernatants, whereas Co-IP detected associated protein complexes in co-culture lysates and did not directly measure ligand–receptor binding at the intact cell surface. Fifth, the context-dependent changes in total CYLD abundance under OGD/R require further investigation and may not directly represent CYLD recruitment or enzymatic activity. Sixth, regional cerebral blood flow was not monitored during MCAO/R surgery, although neurological deficit criteria and TTC staining were used to confirm ischemic injury. Finally, quantitative assessment of primary microglial purity and baseline activation was not performed, which may limit the characterization of the *in vitro* culture system.

6. Conclusions

In summary, our findings indicate that SPATA2 may limit inflammatory damage after focal cerebral ischemia/reperfusion and is associated with changes in selected microglial inflammatory markers within the peri-

ischemic cortex. *In vitro*, neuron-derived SPATA2 regulated microglial inflammatory responses in a Transwell neuron–microglia co-culture system. At the mechanistic level, these results are consistent with a model in which SPATA2 affects CYLD-related NF-κB/CX3CR1 signaling and soluble CX3CL1 release. However, additional *in vivo* studies are needed to clarify the causal sequence of this pathway.

Abbreviations

CNS, central nervous system; Co-IP, co-immunoprecipitation; CX3CL1, C-X-C motif 3 chemokine ligand 1; CX3CR1, CX3C chemokine receptor 1; CYLD, cylindromatosis; DUB, deubiquitinase; HOIL-1, heme-oxidized IRP2 ubiquitin ligase 1-like; HOIP, HOIL-1L interacting protein; Iba1, ionized calcium binding adaptor molecule 1; IL-1β, interleukin-1 beta; LUBAC, linear ubiquitin chain assembly complex; MCAO/R, middle cerebral artery occlusion/reperfusion; NF-κB, nuclear factor-κB; NLRP3, NOD-like receptor family, pyrin domain containing 3; OGD/R, oxygen-glucose deprivation; RT-qPCR, real-time quantitative polymerase chain reaction; SHARPIN, shank-associated RH domain interacting protein; TNF-α, tumor necrosis factor alpha.

Availability of Data and Materials

All data generated or analyzed during this study are included in this published article and its **Supplementary Material**.

Author Contributions

JJ designed the study, performed the experiment, acquired and analyzed the data, performed the statistical analysis and drafted the manuscript. YehD, JJ, WY and XL handled the funding. YehD and WY conceived part of the experimental schemes, supervised all the experiments, interpreted experimental results and provided the critical revision of the manuscript. XL and YexD performed part of the experiment, provided key reagents and materials supporting data acquisition of this study. All authors contributed to editorial changes in the manuscript. All authors read and approved the final manuscript. All authors have participated sufficiently in the work and agreed to be accountable for all aspects of the work.

Ethics Approval and Consent to Participate

Our manuscript data were collected from animals and the study was approved by the Ethics Committee for Animal Experimentation of Chongqing Medical University (IACUC-CQMU-2025-02042). All animal procedures were conducted according to the National Institutes of Health Guide for the Care and Use of Laboratory Animals. Randomized grouping and blinded analysis were implemented during all experimental procedures. The reporting of this study follows the ARRIVE 2.0 guidelines.

Acknowledgment

Not applicable.

Funding

This study was funded by the Natural Science Foundation of Chongqing (CSTB2023NSCQ-MSX0263), the National Natural Science Foundation of China (82371194 and 82602355), the Natural Science Foundation of Chongqing Municipality (2022NSCQ-LZX0010 and CSTB2024NSCQ-QCXMX0004), the Science and Technology Research Program of Chongqing Municipal Education Commission (KJQN202201803) and Chongqing University of Humanities and Science Research Project (CRKZK2022010).

Conflicts of Interest

The authors declare no conflicts of interest.

Declaration of AI and AI-Assisted Technologies in the Writing Process

During the preparation of this work, the authors used ChatGpt-5.2 in order to check spelling and grammar. After using this tool, the authors reviewed and edited the content as needed and take full responsibility for the content of the publication.

Supplementary Material

Supplementary material associated with this article can be found, in the online version, at https://doi.org/10.31083/JIN51769.

References

[1] Jolugbo P, Ariëns RAS. Thrombus Composition and Efficacy of Thrombolysis and Thrombectomy in Acute Ischemic Stroke. Stroke. 2021; 52: 1131–1142. https://doi.org/10.1161/STROKEAHA.120.032810

[2] Ho JP, Powers WJ. Contemporary Management of Acute Ischemic Stroke. Annual Review of Medicine. 2025; 76: 417–429. https://doi.org/10.1146/annurev-med-050823-094312

[3] Kauw F, Bennink E, de Jong HWAM, Kappelle LJ, Horsch AD, Velthuis BK, et al. Intracranial Cerebrospinal Fluid Volume as a Predictor of Malignant Middle Cerebral Artery Infarction. Stroke. 2019; 50: 1437–1443. https://doi.org/10.1161/STROKEAHA.119.024882

[4] Levinson S, Pulli B, Heit JJ. Neuroinflammation and acute ischemic stroke: impact on translational research and clinical care. Frontiers in Surgery. 2025; 12: 1501359. https://doi.org/10.3389/fsurg.2025.1501359

[5] Jin WN, Shi SXY, Li Z, Li M, Wood K, Gonzales RJ, et al. Depletion of microglia exacerbates postischemic inflammation and brain injury. Journal of Cerebral Blood Flow and Metabolism: Official Journal of the International Society of Cerebral Blood Flow and Metabolism. 2017; 37: 2224–2236. https://doi.org/10.1177/0271678X17694185

[6] Abe N, Nishihara T, Yorozuya T, Tanaka J. Microglia and Macrophages in the Pathological Central and Peripheral Nervous Systems. Cells. 2020; 9: 2132. https://doi.org/10.3390/cells9092132
[7] Chan TYH, Ma BDY, Hung TK, Wong JSY, Lo BWY. Microglial Polarization and Therapeutic Strategies in Post-stroke Neuroinflammation. Neurology and Therapy. 2025; 14: 2277–2293. https://doi.org/10.1007/s40120-025-00825-8
[8] Paolicelli RC, Sierra A, Stevens B, Tremblay ME, Aguzzi A, Ajami B, et al. Microglia states and nomenclature: A field at its crossroads. Neuron. 2022; 110: 3458–3483. https://doi.org/10.1016/j.neuron.2022.10.020
[9] Pawelec P, Ziemka-Nalecz M, Sypecka J, Zalewska T. The Impact of the CX3CL1/CX3CR1 Axis in Neurological Disorders. Cells. 2020; 9: 2277. https://doi.org/10.3390/cells9102277
[10] Subbarayan MS, Joly-Amado A, Bickford PC, Nash KR. CX3CL1/CX3CR1 signaling targets for the treatment of neurodegenerative diseases. Pharmacology & Therapeutics. 2022; 231: 107989. https://doi.org/10.1016/j.pharmthera.2021.107989
[11] Jiang L, Zhang X, Wang S, Zhang J, Chen J, Lu J, et al. Functional Monomers Equipped Microgel System for Managing Parkinson's Disease by Intervening Chemokine Axis-mediated Nerve Cell Communications. Advanced Science (Weinheim, Baden-Wurttemberg, Germany). 2025; 12: e2410070. https://doi.org/10.1002/advs.202410070
[12] Galán-Ganga M, García-Yagüe ÁJ, Lastres-Becker I. Role of MSK1 in the Induction of NF-κB by the Chemokine CX3CL1 in Microglial Cells. Cellular and Molecular Neurobiology. 2019; 39: 331–340. https://doi.org/10.1007/s10571-019-00664-w
[13] Zhuang Q, Ou J, Zhang S, Ming Y. Crosstalk between the CX3CL1/CX3CR1 Axis and Inflammatory Signaling Pathways in Tissue Injury. Current Protein & Peptide Science. 2019; 20: 844–854. https://doi.org/10.2174/1389203720666190305165722
[14] Chamera K, Trojan E, Szuster-Głuszczak M, Basta-Kaim A. The Potential Role of Dysfunctions in Neuron-Microglia Communication in the Pathogenesis of Brain Disorders. Current Neuropharmacology. 2020; 18: 408–430. https://doi.org/10.2174/1570159X17666191113101629
[15] He Q, Zhou T, He Q. Targeting CX3CR1 Signaling Dynamics: A Critical Determinant in the Temporal Regulation of Post-Stroke Neurorepair. Brain Sciences. 2025; 15: 759. https://doi.org/10.3390/brainsci15070759
[16] Ohtake F, Saeki Y, Ishido S, Kanno J, Tanaka K. The K48-K63 Branched Ubiquitin Chain Regulates NF-κB Signaling. Molecular Cell. 2016; 64: 251–266. https://doi.org/10.1016/j.molcel.2016.09.014
[17] Lork M, Verhelst K, Beyaert R. CYLD, A20 and OTULIN deubiquitinases in NF-κB signaling and cell death: so similar, yet so different. Cell Death and Differentiation. 2017; 24: 1172–1183. https://doi.org/10.1038/cdd.2017.46
[18] Lee BC, Miyata M, Lim JH, Li JD. Deubiquitinase CYLD acts as a negative regulator for bacterium NTHi-induced inflammation by suppressing K63-linked ubiquitination of MyD88. Proceedings of the National Academy of Sciences of the United States of America. 2016; 113: E165–E171. https://doi.org/10.1073/pnas.1518615113
[19] Jiang J, Luo Y, Qin W, Ma H, Li Q, Zhan J, et al. Electroacupuncture Suppresses the NF-κB Signaling Pathway by Upregulating Cylindromatosis to Alleviate Inflammatory Injury in Cerebral Ischemia/Reperfusion Rats. Frontiers in Molecular Neuroscience. 2017; 10: 363. https://doi.org/10.3389/fnmol.2017.00363
[20] Elliott PR, Leske D, Hrdinka M, Bagola K, Fiil BK, McLaughlin SH, et al. SPATA2 Links CYLD to LUBAC, Activates CYLD, and Controls LUBAC Signaling. Molecular Cell. 2016; 63: 990–1005. https://doi.org/10.1016/j.molcel.2016.08.001
[21] Takiuchi T, Nakagawa T, Tamiya H, Fujita H, Sasaki Y, Saeki Y, et al. Suppression of LUBAC-mediated linear ubiquitination by a specific interaction between LUBAC and the deubiquitinases CYLD and OTULIN. Genes to Cells: Devoted to Molecular & Cellular Mechanisms. 2014; 19: 254–272. https://doi.org/10.1111/gtc.12128
[22] Gao L, Zhang W, Shi XH, Chang X, Han Y, Liu C, et al. The mechanism of linear ubiquitination in regulating cell death and correlative diseases. Cell Death & Disease. 2023; 14: 659. https://doi.org/10.1038/s41419-023-06183-3
[23] Douanne T, Chapelier S, Rottapel R, Gavard J, Bidère N. The LUBAC participates in lysophosphatidic acid-induced NF-κB activation. Cellular Immunology. 2020; 353: 104133. https://doi.org/10.1016/j.cellimm.2020.104133
[24] Schlicher L, Brauns-Schubert P, Schubert F, Maurer U. SPATA2: more than a missing link. Cell Death and Differentiation. 2017; 24: 1142–1147. https://doi.org/10.1038/cdd.2017.26
[25] Maran C, Tassone E, Masola V, Onisto M. The Story of SPATA2 (Spermatogenesis-Associated Protein 2): From Sertoli Cells to Pancreatic Beta-Cells. Current Genomics. 2009; 10: 361–363. https://doi.org/10.2174/138920209788920976
[26] Ren Y, Jiang J, Jiang W, Zhou X, Lu W, Wang J, et al. Spata2 Knockdown Exacerbates Brain Inflammation via NF-κB/P38MAPK Signaling and NLRP3 Inflammasome Activation in Cerebral Ischemia/Reperfusion Rats. Neurochemical Research. 2021; 46: 2262–2275. https://doi.org/10.1007/s11064-021-03360-8
[27] Elliott PR, Leske D, Wagstaff J, Schlicher L, Berridge G, Maslen S, et al. Regulation of CYLD activity and specificity by phosphorylation and ubiquitin-binding CAP-Gly domains. Cell Reports. 2021; 37: 109777. https://doi.org/10.1016/j.celrep.2021.109777
[28] Yang XD, Li W, Zhang S, Wu D, Jiang X, Tan R, et al. PLK4 deubiquitination by Spata2-CYLD suppresses NEK7-mediated NLRP3 inflammasome activation at the centrosome. The EMBO Journal. 2020; 39: e102201. https://doi.org/10.15252/embj.2019102201
[29] Schlicher L, Wissler M, Preiss F, Brauns-Schubert P, Jakob C, Dumit V, et al. SPATA2 promotes CYLD activity and regulates TNF-induced NF-κB signaling and cell death. EMBO Reports. 2016; 17: 1485–1497. https://doi.org/10.15252/embr.201642592
[30] Longa EZ, Weinstein PR, Carlson S, Cummins R. Reversible middle cerebral artery occlusion without craniectomy in rats. Stroke. 1989; 20: 84–91. https://doi.org/10.1161/01.str.20.1.84
[31] Lian H, Roy E, Zheng H. Protocol for Primary Microglial Culture Preparation. Bio-protocol. 2016; 6: e1989. https://doi.org/10.21769/BioProtoc.1989
[32] Zhao Y, Xiao C, Chen H, Zhu R, Zhang M, Liu H, et al. Single-Cell RNA-Seq Reveals Changes in Cell Subsets in the Cortical Microenvironment during Acute Phase of Ischemic Stroke Rats. Journal of Integrative Neuroscience. 2023; 22: 128. https://doi.org/10.31083/j.jin2205128
[33] Lyu J, Xie D, Bhatia TN, Leak RK, Hu X, Jiang X. Microglial/Macrophage polarization and function in brain injury and repair after stroke. CNS Neuroscience & Therapeutics. 2021; 27: 515–527. https://doi.org/10.1111/cns.13620
[34] Planas AM. Role of microglia in stroke. Glia. 2024; 72: 1016–1053. https://doi.org/10.1002/glia.24501
[35] Lv J, Jiao Y, Zhao X, Kong X, Chen Y, Li L, et al. Examining the Impact of Microglia on Ischemic Stroke With an Emphasis on the Metabolism of Immune Cells. CNS Neuroscience & Therapeutics. 2025; 31: e70229. https://doi.org/10.1111/cns.70229
[36] Shi Y, Yang Y, Liu J, Zheng J. Avicularin Treatment Ameliorates

Ischemic Stroke Damage by Regulating Microglia Polarization and its Exosomes via the NLRP3 Pathway. Journal of Integrative Neuroscience. 2024; 23: 196. https://doi.org/10.31083/j.jin2311196

[37] Zhang Y, Lian L, Fu R, Liu J, Shan X, Jin Y, et al. Microglia: The Hub of Intercellular Communication in Ischemic Stroke. Frontiers in Cellular Neuroscience. 2022; 16: 889442. https://doi.org/10.3389/fncel.2022.889442

[38] Yang S, Chen Y, Tang J, Cui Y, Wei W, Hao Z, et al. Microglia-astrocyte crosstalk following ischemic stroke. Molecular Brain. 2025; 18: 75. https://doi.org/10.1186/s13041-025-01244-4

[39] Marín-Rubio JL, Raote I, Inns J, Dobson-Stone C, Rajan N. CYLD in health and disease. Disease Models & Mechanisms. 2023; 16: dmm050093. https://doi.org/10.1242/dmm.050093

[40] Zhan L, Qiu M, Zheng J, Lai M, Lin K, Dai J, et al. Fractalkine/CX3CR1 axis is critical for neuroprotection induced by hypoxic postconditioning against cerebral ischemic injury. Cell Communication and Signaling: CCS. 2024; 22: 457. https://doi.org/10.1186/s12964-024-01830-4